Increase of Palmitic Acid Concentration Impairs Endothelial Progenitor Cell and Bone Marrow–Derived Progenitor Cell Bioavailability

Role of the STAT5/PPARγ Transcriptional Complex

Antonella Trombetta,[1] Gabriele Togliatto,[1] Arturo Rosso,[1] Patrizia Dentelli,[1] Cristina Olgasi,[1] Paolo Cotogni,[2] and Maria Felice Brizzi[1]

Metabolic profiling of plasma nonesterified fatty acids discovered that palmitic acid (PA), a natural peroxisome proliferator–activated receptor γ (PPARγ) ligand, is a reliable type 2 diabetes biomarker. We investigated whether and how PA diabetic (*d*-PA) concentrations affected endothelial progenitor cell (EPC) and bone marrow–derived hematopoietic cell (BM-HC) biology. PA physiologic (*n*-PA) and *d*-PA concentrations were used. Proliferating cell nuclear antigen content and signal transducer and activator of transcription 5 (STAT5), PPARγ, cyclin D1, and $p21^{Waf}$ expression were evaluated. Small interfering RNA technology, gene reporter luciferase assay, electrophoretic mobility shift assay, chromatin immunoprecipitation assay, and coimmunoprecipitation were exploited. In vivo studies and migration assays were also performed. *d*-PA, unlike *n*-PA or physiological and diabetic oleic and stearic acid concentrations, impaired EPC migration and EPC/BM-HC proliferation through a PPARγ-mediated STAT5 transcription inhibition. This event did not prevent the formation of a STAT5/PPARγ transcriptional complex but was crucial for gene targeting, as $p21^{Waf}$ gene promoter, unlike cyclin D1, was the STAT5/PPARγ transcriptional target. Similar molecular events could be detected in EPCs isolated from type 2 diabetic patients. By expressing a constitutively activated STAT5 form, we demonstrated that STAT5 content is crucial for gene targeting and EPC fate. Finally, we also provide in vivo data that *d*-PA–mediated EPC dysfunction could be rescued by PPARγ blockade. These data provide first insights on how mechanistically *d*-PA drives EPC/BM-HC dysfunction in diabetes. ***Diabetes*** **62:1245–1257, 2013**

Metabolomic, a recent tool exploited to explore the complex interactions of metabolites in livelihood systems, discloses the metabolic response to pathophysiologic stimuli or genetic alterations (1). In recent years, metabolomic has been fruitfully applied in clinical settings, including diabetes (2,3). In type 2 diabetes, alteration of lipid and, in particular, of fatty acid metabolism is a common feature (4). A linear correlation among blood glucose levels, hepatic glucose production, and nonesterified fatty acid (NEFA) plasma levels has been reported in diabetes (4). Indeed, total NEFA is considered an important index for type 2 diabetes diagnosis (5). Recently, metabolic profiling of plasma NEFAs in type 2 diabetic patients has discovered different biomarkers, and palmitic acid (PA), a 16-carbon saturated fatty acid, accounting for ~30% of total plasma NEFAs (6), has been considered a reliable one (3,5).

NEFAs act both as ligands for cell-surface receptors (e.g., G-protein–coupled receptors) and for transcription factor receptors as peroxisome proliferator–activated receptors (PPARs). PPARs are crucial transcriptional regulators of genes involved in glycemic control, lipid metabolism, and inflammation (7). Three different PPAR isoforms characterized by unique functions and denoted as α, β/δ, and γ have been described (8). PPARγ, a key mediator in adipogenesis (9), lipid metabolism (10), and glucose homeostasis (11), also controls target genes involved in vascular biology and diabetes-associated vascular complications (8,12). Cardiovascular risk factors, such as diabetes, reduce endothelial progenitor cell (EPC) bioavailability by impairing their mobilization, proliferation, and integration into injured vascular sites, crucial events for vessel repair (13). In recent years, evidence for PPARγ-mediated vascular protection in diabetic patients has been provided (14). A great deal of interest on PPARγ agonists was generated by the finding that they can avoid progression of vascular disease by improving EPC functions (15). However, whether such effect depends on a direct action on EPCs and/or on their effect on glucose metabolism is still debated (16). Moreover, as in type 2 diabetes NEFA concentrations (17) and changes in EPC number and functional capability are closely associated with cardiovascular risk factor profile (13,18), whether NEFA concentrations, by triggering PPARγ activity, impact on EPC bioavailability is still an unsolved issue (19,20).

PPARγ mainly forms heterodimers with the nuclear retinoid X receptor-α (8) and binds to PPAR response elements in the regulatory regions of target genes (21). Moreover, PPARγ also forms a transcriptional complex with the signal transduction and activator of transcription 5 (STAT5) to control EPC cell-cycle progression (22). However, agonist-dependent, unlike agonist-independent, PPARγ expression led to impaired hematopoietic progenitor functions (23), and inhibition of EPC proliferation (19,20). Thus, physiological PPARγ agonists, as PA, by impairing EPC bioavailability, can actually contribute to vascular damage in a diabetic setting.

In the current study, we investigated whether and how mechanistically high plasma levels of PA could affect EPC

From the [1]Department of Medical Sciences, University of Turin, Turin, Italy; and the [2]Department of Anesthesiology and Intensive Care, University of Turin, Turin, Italy.
Corresponding author: Maria Felice Brizzi, mariafelice.brizzi@unito.it.
Received 22 May 2012 and accepted 4 October 2012.
DOI: 10.2337/db12-0646
This article contains Supplementary Data online at http://diabetes.diabetesjournals.org/lookup/suppl/doi:10.2337/db12-0646/-/DC1.

bioavailability and possibly contribute to diabetes-associated vascular damage.

RESEARCH DESIGN AND METHODS

Reagents. A detailed list of the reagents and antibodies used in this study is reported in Supplementary Table 1.

Diabetic subjects and healthy donors. Whole blood was recovered from 14 individuals with type 2 diabetes selected at the diagnosis (two independent fasting glucose determinations) and from 14 sex- and age-matched healthy donors. Four additional longstanding diabetic patients were enrolled. Data relative to patients and control subjects are reported in Table 1. Ethical approval was obtained from Servizio Immunoematologia e Medicina Trasfusionale, Azienda Ospedaliera Ospedale Infantile Regina Margherita Sant Anna (Torino, Italy). Informed consent was obtained in accordance with the Declaration of Helsinki.

Isolation and culture of EPCs and endothelial cells. Isolation and characterization of EPCs and mature endothelial cells (ECs) were performed as described (24,25). To isolate EPCs, peripheral blood mononuclear cells were obtained by Ficoll Histopaque 1077 and plated onto collagen-1–coated dishes. Fluorescence-activated cell sorting (FACS) analysis was used to characterize EPC surface markers. At day 14, cells were depleted with serum-free medium for 12 h and then challenged with EGM-2 medium containing PA, 100 μmol/L physiologic PA (*n*-PA) or 300 μmol/L diabetic PA (*d*-PA), and ethanol-BSA (not exceeding 0.15% and 0.003% final concentration, respectively) as control. In selected experiments, oleic acid (OA) and stearic acid (SA) at the same molar concentrations were used.

Isolation of bone marrow–derived hemopoietic cells and CFU assay. Bone marrow (BM)–derived hemopoietic cells (an additional model of immature cells) were obtained from murine bone marrow flushed from the femurs and tibiae of 10–12-week-old FVB mice and isolated by Ficoll Histopaque 1083. CD117/c-kit$^+$ cells were sorted with the CD117 magnetic MicroBeads Kit (Miltenyi Biotec, Bergisch Gladbach, Germany) following the manufacturer's protocol. Sorted cells were seeded (1×10^5 cells/mL) (BM-CD117$^+$) in methylcellulose containing complete medium and cultured for 15 days. Ethanol-BSA was used as control. At the end of the experiments, individual colonies (>100 cells) were counted with a scoring grid using an inverted microscope.

Preparation of fatty acid–albumin complexes. Saturated PA and SA or monounsaturated OA were used. Lipid-containing media were prepared by conjugating free fatty acids with BSA using a modified method described by Svedberg et al. (26). Preliminary experiments were performed with delipidated sera as described by Cham and Knowles (27). Because no significant differences were observed in pilot experiments, nondelipidated sera were used throughout the study.

Migration assay. EPC migration was performed in Boyden's chambers as previously described (28).

TABLE 1
Data referred to diabetic patients and healthy subjects

	Diabetic patients	Healthy subjects	LS diabetic patients
Sex (male/female)	6/8	7/7	2/2
Age (years)	51.3 ± 8.74	45.3 ± 3.96	55.6 ± 5.38
HbA_{1c} (%)	7.9 ± 1.5	5.4 ± 1.3	8.1 ± 1.7
Fasting glucose (mmol/L)	9.6 ± 1.69	6.21 ± 0.58	10.3 ± 1.94
Triglycerides (mmol/L)	1.86 ± 0.54	1.52 ± 0.64	1.98 ± 0.73
Total cholesterol (mmol/L)	6.81 ± 1.78	4.24 ± 0.97	7.01 ± 2.09
LDL cholesterol (mmol/L)	4.92 ± 1.6	1.19 ± 0.23	5.16 ± 1.65
HDL cholesterol (mmol/L)	1.04 ± 0.21	2.75 ± 0.71	0.95 ± 0.75
Cholesterol/ apolipoprotein B	1.1 ± 0.5	1.7 ± 0.4	1.1 ± 0.9
Plasma NEFA (g/L)	0.45 ± 0.21	0.18 ± 0.09	0.46 ± 0.11
BMI	26.7 ± 2.6	24.2 ± 1.85	26.9 ± 2.9

Data are presented as mean ± SD unless otherwise specified. LS, long-standing.

Reactive oxygen species generation and senescence. Reactive oxygen species generation and senescence were evaluated as previously described (25,28).

Cell-cycle progression and proliferation assay. Cell-cycle progression was evaluated by FACS analysis (22). The percentage of cells in each cell-cycle phase was determined by ModFit LT software (Verity Software House, Inc., Topsham, ME). Cell proliferation was also assayed by direct cell count by three different operators and by evaluating the percentage of proliferating cell nuclear antigen (PCNA)-positive cells by FACS analysis.

Western blotting and coimmunoprecipitation. Western blotting (WB) analysis and coimmunoprecipitation (co-IP) experiments on EPCs treated as indicated were performed as previously described (22,28,29). Images were acquired with a Bio-Rad GS 250 molecular imager (Bio-Rad, Hercules, CA), and densitometric analysis was performed using the software ImageJ 1.45 m (National Institutes of Health).

RNA isolation and quantitative real-time PCR. Quantitative real-time polymerase chain reactions (q-RT-PCRs) were performed as described (28,29). Primers are reported in Supplementary Table 2.

Bioinformatic analysis. Bioinformatic analysis of putative response elements on *Homo sapiens* STAT5 gene (AC_099811), *Homo sapiens* cyclin D1 promoter (Z29078.1), *Homo sapiens* $p21^{Waf}$ (NG_009364.1), *Mus musculus* cyclinD1 (sequence NC_000073) gene, and *Mus musculus* $p21^{Waf}$ (sequence NC_000083) were performed using the following software: NHRScan (http://asp.ii.uib.no:8090/cgi-bin/NHR-scan/nhr_scan.cgi) for the PPAR putative response element (PPRE) sequence and Motif (http://www.genome.jp/tools/motif/) for STAT5 response elements. The results were then verified with Transcription Element Search Software (http://agave.humgen.upenn.edu/utess/tess).

Chromatin immunoprecipitation. Chromatin immunoprecipitation (ChIP) assay was performed using a Magna ChIP kit (Millipore, Temecula, CA) (22). Primers are reported in Supplementary Table 2.

Electrophoretic mobility shift assay. Nuclear extracts were prepared as previously described (22,30). Oligonucleotides used are reported in Supplementary Table 2.

Endogenous depletion of PPARγ by small interfering RNA. EPCs were transiently transfected with specific PPARγ small interfering RNA (siRNA) and with duplex siRNAs as scramble controls, purchased from Qiagen (Valencia, CA) (22).

Constitutively activated STAT5 form transfection. Fifteen-day–cultured EPCs were transiently transfected with a plasmid constitutively activated STAT5 form (STAT1*6) or the empty vector pCNeo as described (22,31).

Luciferase gene reporter and site-directed mutagenesis. The luciferase reporter assay was performed using three different constructs generated by subcloning into restriction sites of the luciferase reporter vector pGL3 Basic Vector (Promega, Madison, WI) two different sequences of the human STAT5A promoter region, amplified using TaKaRa LA Taq (Takara Bio-Europe SAS, Saint-German-en-Laye, France) from human genomic DNA. All fragments were inserted to obtain three different plasmids: pGL3-A3, pGL3-Inter2, and pGL3-Inter2-A3. A site-direct mutagenesis on the latter plasmid was performed as described by Weiner et al. (32). Primers are reported in Supplementary Table 2.

Vasculogenetic assay. EPC vasculogenic capability was evaluated in vitro and in vivo as previously described (28,29,33).

Statistical analysis. Comparison and significance of differences between two groups was performed with the *t* test. Comparison among three or more groups was performed with one-way ANOVA, and significance of differences was evaluated with the Newman-Keuls multicomparison posttest. The *P* values <0.05 were considered significant and indicated with different symbols as detailed in the figure legends. All statistical analyses were carried out with GraphPad Prism version 5.04 software (GraphPad Software, Inc.).

RESULTS

Diabetic concentrations of PA impair EPC functions. In diabetic patients, plasmatic PA concentration rises up to three- to fivefold when compared with matched healthy subjects (34) and seems to impair EPC functions (19,20). We attempted to investigate the molecular mechanisms accounting for this effect. EPCs were characterized and PA dose-response experiments performed (Supplementary Figs. 1 and 2) by evaluating the expression of two cell-cycle regulatory proteins: cyclin D1 and $p21^{waf}$ (25). We demonstrated that only for doses greater than or equal to PA 300 μmol/L, diabetic concentrations (*d*-PA), cyclin D1 and $p21^{waf}$ content changed. Parallel experiments performed with physiological and diabetic SA concentrations demonstrated that such saturated fatty acid had no significant effect on cell-cycle regulatory proteins and EPC proliferation

and migration (Supplementary Fig. 3). To validate the biological relevance of these results, EPCs were cultured with physiological (100 μmol/L *n*-PA) or *d*-PA concentrations. As shown in Fig. 1*A*, only *d*-PA treatment induced a decrease in the number of cells. Cell-cycle analysis (Fig. 1*B*) demonstrated that this effect is not associated with cell death (Supplementary Fig. 4*A*–*C*). Cytofluorimetric analysis of PCNA (Fig. 1*C*) and expression of cyclin D1 and p21^{Waf} are consistent (Fig. 1*D* and *E*). *d*-PA did not induce ROS generation and EPC senescence (Supplementary Fig. 4*D* and *E*). Moreover, impaired EPC migratory capability was detected upon *d*-PA treatment (Fig. 1*F*). Conversely, *d*-PA did not affect mature EC proliferation and migration (Supplementary Fig. 5).

Beneficial effects are exerted by monounsaturated fatty acid, as OA (35,36). The effects of OA on EPC proliferation and migration were evaluated at physiological (100 μmol/L *n*-OA) and diabetic (300 μmol/L *d*-OA) concentrations. Indeed, *d*-OA concentration had no significant effects on EPC proliferation and migration (Fig. 2*A*, *B*, and *D*). Data were further sustained by cyclin D1 and p21^{Waf} expression (Fig. 2*B*). However, when added to *d*-PA, only *n*-OA rescued *d*-PA–mediated EPC cell-cycle arrest and migration (Fig. 2*C*–*E*).

_d_-PA induces PPARγ expression and downregulation of STAT5A transcription. Although both IL-3 and synthetic or natural PPARγ agonists activate PPARγ expression, only IL-3 induced EPC expansion via the formation of a STAT5/PPARγ transcriptional complex (22,29). PA is natural PPARγ agonist (37,38), thus the effect of *d*-PA and *n*-PA on PPARγ and STAT5 expression was first evaluated. Accordingly with previous data (22), *d*-PA only induced PPARγ expression and decreased STAT5A expression (Fig. 3*A*–*C*). No changes in STAT5B expression were detected, suggesting that PPARγ directly controls STAT5A transcription (Fig. 3*D*). To validate this possibility, the STAT5 gene promoter was analyzed to find PPREs. Three different regulatory regions have been identified in the human STAT5 gene promoter (39). Regions I and II are putative STAT5A and STAT5B promoters, respectively, whereas region III acts as a negative regulatory element for both genes. Regions I–III contain different functional sequences denoted A1, A2, and A3 (region I) and Inter1 and Inter2 (region III) (39). Consistent with the presence (NHRScan bioinformatic software) of two different putative PPREs in A3 and Inter 2 regions, ChIP analysis demonstrated that PPARγ binds to A3 and the Inter2 regulatory regions of STAT5 promoter (Fig. 3*E*). To further validate this result, the two STAT5 genomic fragments, A3 and Inter 2, were cloned as single fragment or juxtaposed to reproduce the whole regulatory region of the STAT5A gene in the pGL3 luciferase reporter vector and denoted as: pGL-A3, pGL-Inter2, and pGL-Inter2:A3 (Fig. 3*G*). Consistent with ChIP analysis, luciferase assay showed that PPARγ even at low concentrations binds to A3 and positively regulates STAT5 transcription. Conversely, PPARγ binds to Inter2 to negatively regulate STAT5 transcription only in *d*-PA–treated EPCs, expressing pGL-Inter2– or pGL-Inter2:A3–containing regions (Fig. 3*G*). By site-directed mutagenesis, we confirmed that the Inter2

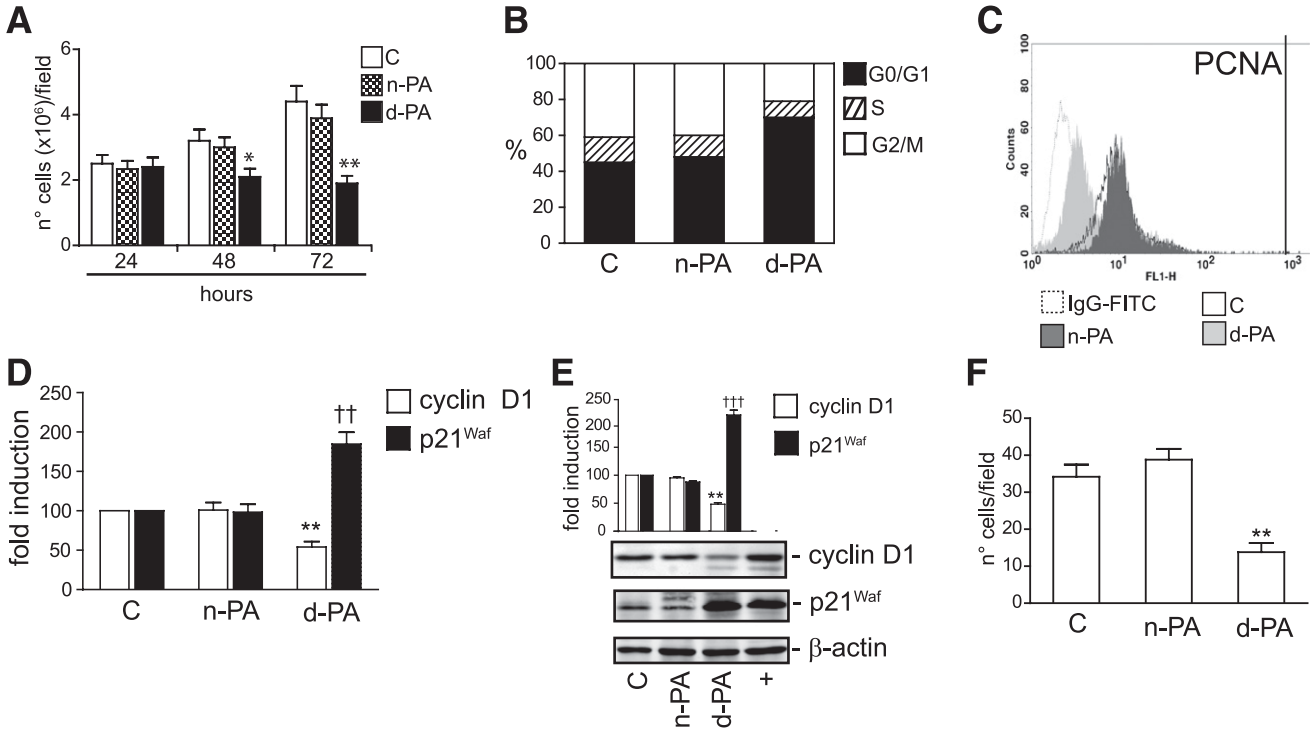

FIG. 1. _d_-PA, unlike _n_-PA, impairs EPC functions. _A_: EPC proliferation in response to the indicated stimuli (data are expressed as mean + SD; $n = 6$; *$P < 0.05$, _d_-PA 48 h vs. C [control] 48 h; **$P < 0.01$, _d_-PA 72 h vs. C 72 h). _B_: FACS analysis indicating the percentage of EPCs at different cell-cycle phases (referred at 48 h) (data are expressed as mean, $n = 6$). _C_: FACS analysis of PCNA-positive EPCs treated as indicated (referred at 48 h). The reported graph is representative of six independent experiments. _D_: q-RT-PCR analysis of cyclin D1 and p21^{Waf} mRNA expression in 48 h–treated EPCs as indicated. Data normalized to the corresponding glyceraldehyde-3-phosphate dehydrogenase mRNA and expressed as mean + SD are reported as fold induction relative to control values arbitrary set as 100 ($n = 9$; **$P < 0.01$, cyclin D1 _d_-PA vs. C and _n_-PA; ††$P < 0.01$, p21^{Waf} _d_-PA vs. C and _n_-PA). _E_: Representative WB and densitometric analysis of cyclin D1 and p21^{Waf} protein content in 48 h–treated EPCs. Densitometric data, normalized to the corresponding β-actin value and expressed as mean + SD, are reported as fold induction relative to control values arbitrarily set as 100 ($n = 9$; **$P < 0.01$, cyclin D1 _d_-PA vs. C and _n_-PA; †††$P < 0.001$, p21^{Waf} _d_-PA vs. C and _n_-PA). IL-3– and AGE-stimulated ECs were used as positive controls for cyclin D1 or p21^{Waf}, respectively. _F_: EPC migration in response to stromal cell–derived factor 1α (SDF-1α) (20 ng/mL). Data are expressed as mean + SD ($n = 6$; **$P < 0.01$, _d_-PA vs. C and _n_-PA).

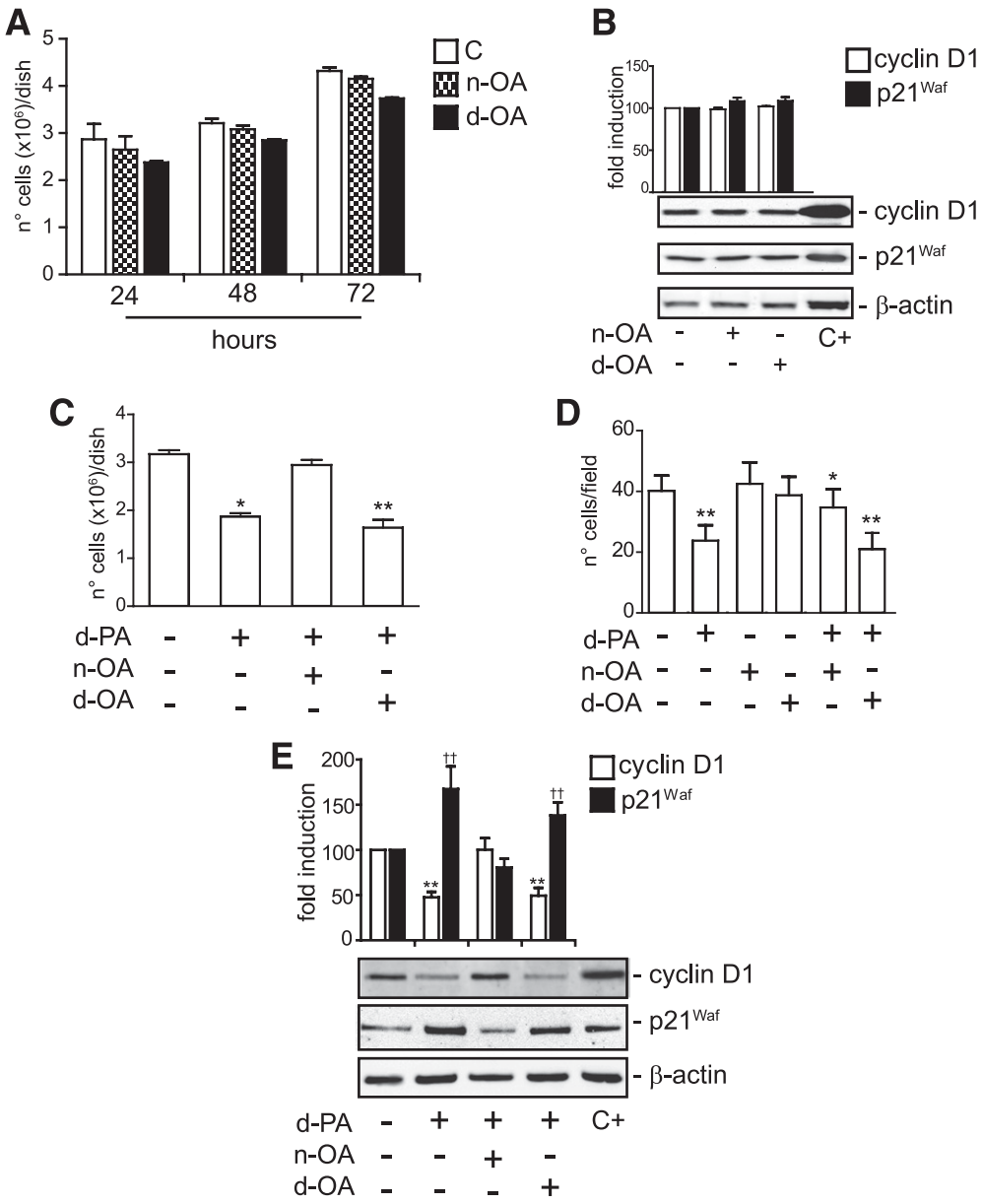

FIG. 2. EPC proliferation and migration upon OA treatment. *A*: Proliferation of EPCs treated as indicated; data are expressed as mean + SD (n = 6). *B*: Representative WB and densitometric analysis of cyclin D1 and p21^{Waf} protein content in 48 h–treated EPCs as indicated; densitometric data normalized to the corresponding β-actin value and expressed as mean + SD are reported as fold induction relative to control values arbitrarily set as 100. *C*: EPC number after 48-h treatment (data are expressed as mean + SD, n = 9; *P < 0.05, *d*-PA vs. no stimulus and *d*-PA + *n*-OA; **P < 0.01, *d*-PA + *d*-OA vs. no stimulus and *d*-PA + *n*-OA). *D*: EPC migration in response to SDF-1α. EPCs were treated for 48 h as indicated. Data are expressed as mean + SD (n = 6; *P < 0.05, *n*-OA + *d*-PA vs. no stimulus, *n*-OA, and *d*-OA; **P < 0.01, *d*-PA and *d*-OA + *d*-PA vs. no stimulus, *n*-OA, and *d*-OA). *E*: Representative WB and densitometric analysis of cyclin D1 and p21^{Waf} protein content in 48 h–treated EPCs as indicated; densitometric data, normalized to the corresponding β-actin values and expressed as mean + SD, are reported as fold induction relative to control values arbitrarily set as 100 (n = 9; **P < 0.01, cyclin D1 *d*-PA and *d*-PA + *d*-OA vs. no stimulus and *d*-PA + *n*-OA; ††P < 0.01, p21^{Waf} *d*-PA and *d*-PA + *d*-OA vs. no stimulus and *d*-PA + *n*-OA). IL-3– and AGE-stimulated ECs were used as positive controls for cyclin D1 or p21^{Waf}, respectively (C+, *B* and *E*).

region is crucial for *d*-PA–mediated inhibition of STAT5A transcription (Fig. 3*G*). Similar results were obtained when electrophoretic mobility shift assay analysis was performed (Fig. 3*F*). By silencing PPARγ, we also demonstrated its biological relevance in mediating inhibition of STAT5A and p21^{Waf} expression, cell-cycle progression, and migration in response to *d*-PA (Supplementary Fig. 6).

Depending on the requested biological response, STAT5–PPARγ complex binds to cyclin D1 or p21^{Waf} gene promoter. To evaluate whether STAT5 formed a complex with PPARγ (22), co-IP experiments were performed. As shown in Fig. 4*A–C*, a STAT5/PPARγ complex containing the activated STAT5A could be detected in *n*-PA– and *d*-PA–treated cells, suggesting that, although at low level of expression, STAT5A (Fig. 4*A*) binds to PPARγ.

Both p21^{Waf} and cyclin D1 promoter regions contain putative response elements for STAT5 and PPARγ (22). Thus, we inquired whether a *d*-PA and *n*-PA–elicited biological response dictates gene targeting. ChIP assay performed on the promoter region of cyclin D1 (22) and on that of p21^{Waf} (Fig. 4*E*) clearly demonstrate that indeed the STAT5/PPARγ complex binds to cyclin D1 or p21^{Waf}

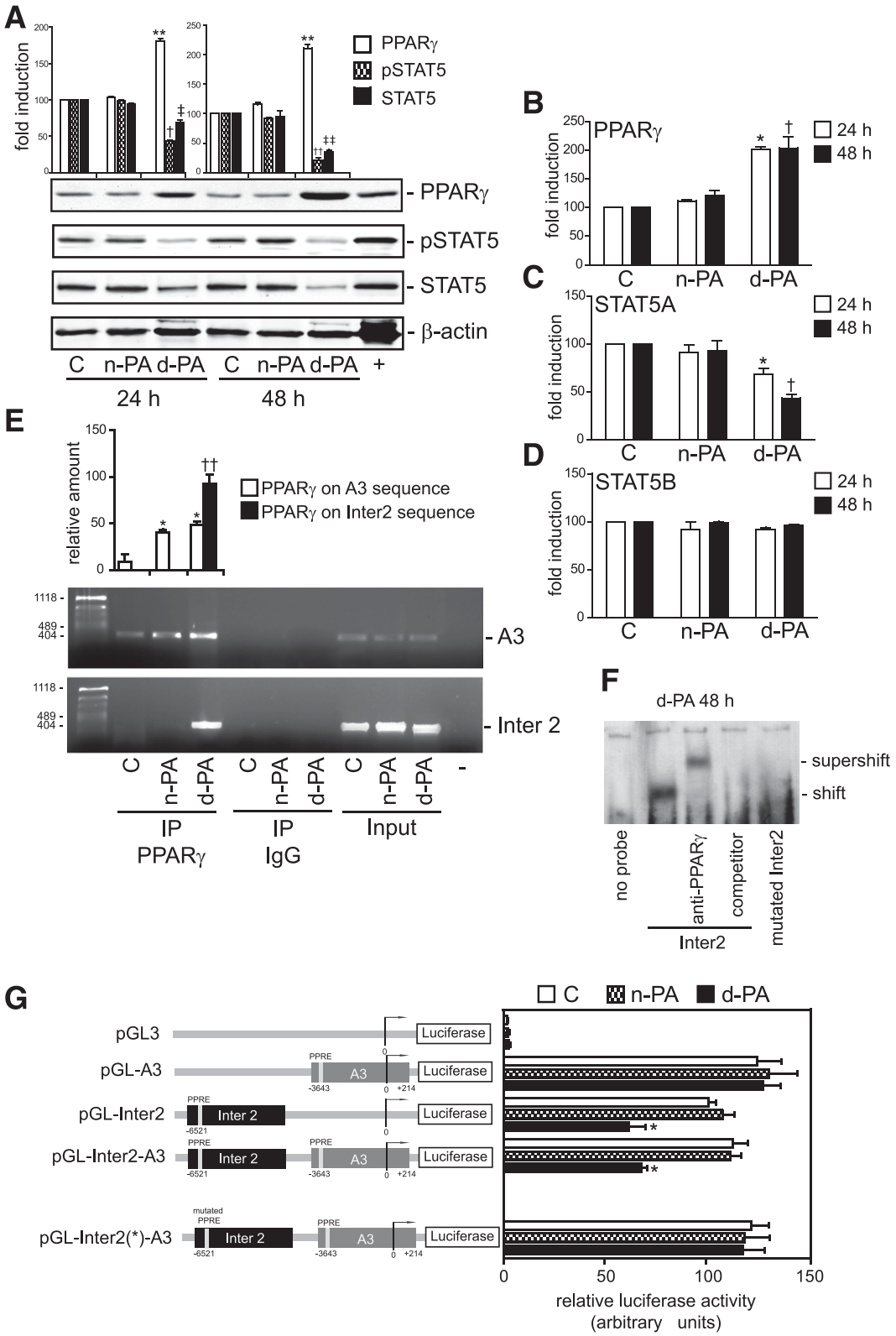

FIG. 3. *d*-PA induces PPARγ expression that leads to STAT5A transcription inhibition. *A*: Representative WB and densitometric analysis of PPARγ, phosphorylated STAT5 (pSTAT5), and STAT5 protein content in EPCs treated for 24 and 48 h as indicated; densitometric data, normalized to the corresponding β-actin values and expressed as mean + SD, are reported as fold induction relative to control values arbitrarily set as 100 (n = 9; **P < 0.01, PPARγ *d*-PA 24 h vs. C (control) 24 h and *n*-PA 24 h and also PPARγ *d*-PA 48 h vs. C 48 h and *n*-PA 48 h; †P < 0.05, pSTAT5 *d*-PA 24 h vs. C 24 h and *n*-PA 24 h; ‡P < 0.05, STAT5: *d*-PA 24 h vs. C 24 h and *n*-PA 24 h; ††P < 0.001, pSTAT5 *d*-PA 48 h vs. C 48 h and *n*-PA 48 h; ‡‡P < 0.001 STAT5 *d*-PA 48 h vs. C 48 h and *n*-PA 48 h). IL-3–stimulated ECs were used as positive control (+). *B*: q-RT-PCR analysis of PPARγ mRNA expression in EPCs treated for 24 and 48 h as indicated; data, normalized to the corresponding GADPH mRNA and expressed as mean + SD, are reported as fold induction relative to control values arbitrarily set as 100 (n = 9; *P < 0.05, *d*-PA 24 h vs. C 24 h and *n*-PA 24 h; †P < 0.05, *d*-PA 48 h vs. C 48 h and *n*-PA 48 h). *C*: q-RT-PCR analysis of STAT5A mRNA expression in EPCs treated for 24 and 48 h as indicated; data, normalized to the corresponding glyceraldehyde-3-phosphate dehydrogenase mRNA and expressed as mean + SD, are reported as fold induction relative to control

promoter depending on the stimulus: it binds to cyclin D1 promoter upon *n*-PA, which does not inhibit EPC cell-cycle progression; conversely, it binds to $p21^{Waf}$ promoter upon *d*-PA that induces EPC cell-cycle arrest. A $p21^{Waf}$/PCNA molecular complex preventing PCNA functional activation has been shown to contribute to cell-cycle arrest (40). Likewise we demonstrated that, in response to *d*-PA only, $p21^{Waf}$ physically interacts with PCNA (Fig. 4*D*).

The relative amount of activated STAT5 regulates EPC progression into the cell cycle. To evaluate whether STAT5 cell content, and in particular its activated form, represents a crucial determinant of EPC fate, EPCs were transiently transfected with STAT1*6 (31) or with the empty vector pCNeo. As shown in Fig. 5*A*, when phosphorylated STAT5 (pSTAT5) content increased, it led to cyclin D1 expression and EPC proliferation (Fig. 5*B–D*) even in the presence of *d*-PA. Consistently, ChIP analysis demonstrated that the increased level of activated STAT5 led the STAT5/PPARγ transcriptional complex to move from the $p21^{Waf}$ gene promoter to that of cyclin D1 (Fig. 5*E*).

We have previously demonstrated that cultured diabetic EPCs are unable to undergo cell proliferation (25,28). To assess the biological relevance of the above results, PPARγ, STAT5, and pSTAT5 levels in EPCs isolated from diabetic patients at diagnosis (*d*-EPCs), from longstanding diabetic patients (LS-dEPCs), showing similar NEFA plasma levels, and from healthy blood donors (hEPCs) were analyzed. The results reported in Fig. 6*A–D* demonstrated that, compared with h-EPCs, *d*-EPCs and LS-dEPCs expressed high PPARγ levels, low STAT5A levels, and a barely detectable level of pSTAT5. To further validate these data, the expression of cyclin D1 and $p21^{Waf}$ was evaluated. The results in Fig. 6*E–H* demonstrated that *d*-EPCs and LS-dEPCs, as *d*-PA–treated cells, expressed high levels of $p21^{Waf}$ and low levels of cyclin D1. ChIP assay further confirmed these results, as in hEPCs, STAT5A and PPARγ were both present on the putative response element of cyclin D1 gene promoter, whereas in *d*-EPCs and LS-dEPCs, both proteins were on the $p21^{Waf}$ gene promoter response element (Fig. 6*I*). When parallel experiments were performed by adding 10 mmol/L glucose to *d*-PA, we found that the decrease in STAT5A and of $p21^{Waf}$ expression correlated with STAT5/PPARγ binding to the $p21^{Waf}$ gene promoter and to EPC proliferation and migration (Supplementary Fig. 7). Pioglitazone improves EPC function in type 2 diabetic patients (15). Consistently, we found that it was able to restore *d*-EPC migration and reduce the percentage of senescent cells, effects not related to STAT5A and PPARγ content (Supplementary Fig. 8).

***d*-PA effects on BM-$CD117^+$ cells and EPC vasculogenic capability.** Different PPARγ agonists inhibit $CD34^+$ colony formation, an effect reverted by GW9662, a specific PPARγ inhibitor (23). To investigate whether *d*-PA also affects BM-derived hematopoietic cell colony formation, BM-$CD117^+$ cells were used. Data in Fig. 7*A* show that $CD117^+$ clonogenic activity was inhibited by *d*-PA treatment, and GW9662 rescued this effect. These data were further supported by cyclin D1 and $p21^{Waf}$ expression (Fig. 7*C*). Moreover, consistent with data obtained in hEPCs, we found that STAT5A expression was reduced only in response to *d*-PA (Fig. 7*B*). Thus, ChIP assay was performed, and the results reported in Fig. 7*D* demonstrate that *d*-PA, unlike *n*-PA, induces the formation of a STAT5/PPARγ transcriptional complex that specifically binds to $p21^{Waf}$ promoter.

The role of PPARγ in mediating EPC dysfunction was also investigated by evaluating EPC vasculogenetic capability (28). Indeed, in vitro and in vivo data demonstrated that *d*-PA–mediated inhibition of EPC vasculogenetic potential could be rescued when the specific PPARγ inhibitor GW9662 was exploited (Fig. 7*E* and *F*).

DISCUSSION

NEFAs and in particular PA and OA are biomarkers of poor metabolic control in diabetic patients (1,2). Among NEFA, PA is a well-known, natural, low-affinity PPAR ligand (41). PPARs belong to the nuclear receptor transcription factor family (8,12). Different PPAR isoforms have been characterized owing to their tissue specificity (8,12), and two diverse variants of PPARγ (1,2) have been described (42). Unlike PPARγ2, PPARγ1 seems to modulate pivotal biological functions in the cardiovascular system (43). Studies to dissect the effects PPARγ agonists, such as pioglitazone, on vascular cells are still debated (15,44,45). We have previously shown that, unlike agonist-independent PPARγ expression, agonist-dependent PPARγ expression inhibits EPC cell-cycle progression (22), suggesting that PPARγ transcriptional activity is much more complex than expected.

PPARγ transcriptional activity mainly depends on the formation of heterodimers with the nuclear retinoid X receptor-α (8). However, we have previously shown that, in IL-3–mediated EPC expansion, PPARγ formed heterodimers with the activated STAT5A to induce cyclin D1 gene transcription (22). STAT5A, in this particular context, transcriptionally controls PPARγ expression (22). In diabetes, multiple factors, such as hyperglycemia, oxidative stress, and advanced glycosylation end products (AGEs), have been investigated as potential mediators of EPC dysfunction (46). Conversely, only few data are so far available on the effects exerted by elevated plasma NEFA concentrations on EPC biology (19,20,47). We report in this study that, consistent with the low ligand affinity of PA for PPARγ, only *d*-PA was able to induce PPARγ expression in EPCs. Moreover, we demonstrated that as the result of its expression/activation, EPCs undergo $p21^{Waf}$-mediated cell-cycle arrest. Moreover, as previously shown (22), we found that *d*-PA–mediated inhibition of EPC progression into the cell cycle is associated with a reduced STAT5A expression.

values arbitrarily set as 100 ($n = 9$; *$P < 0.05$, *d*-PA 24 h vs. C 24 h and *n*-PA 24 h; †$P < 0.05$, *d*-PA 48 h vs. C 48 h and *n*-PA 48 h). *D*: q-RT-PCR analysis of STAT5B mRNA expression in EPCs treated for 24 and 48 h as indicated; data, normalized to the corresponding GADPH mRNA and expressed as mean + SD, are reported as fold induction relative to control values arbitrarily set as 100 ($n = 9$). *E*: Representative ChIP analysis of PPARγ binding to PPRE in A3 and Inter2 sequences of the STAT5A human gene in EPCs treated for 48 h as indicated; densitometric analysis data, normalized to the corresponding Input values and expressed as mean + SD, are reported as relative amount of PCR products ($n = 9$; *$P < 0.05$, PPARγ on A3 sequence *n*-PA and *d*-PA vs. C; ††$P < 0.01$, PPARγ on Inter2 sequence *d*-PA vs. C and *n*-PA). *F*: Electrophoretic mobility shift assay of PPARγ binding specificity to the Inter2 sequence of STAT5A gene promoter in 48 h–treated EPCs with *d*-PA. *G*: Firefly luciferase activity and schematic representation of the different human STAT5A pGL3 gene reporter plasmids transfected in EPCs. EPCs were treated for 48 h as indicated; luminescence data, normalized to the corresponding Renilla luciferase values and expressed in arbitrary units as mean + SD, are reported as relative luciferase activity ($n = 9$; *$P < 0.05$, pGL3-Inter2 and pGL3-Inter2-A3 *d*-PA–treated cells vs. C and *n*-PA–treated cells and also vs. pGL3-Inter2[mutated]-A3 *d*-PA–treated cells).

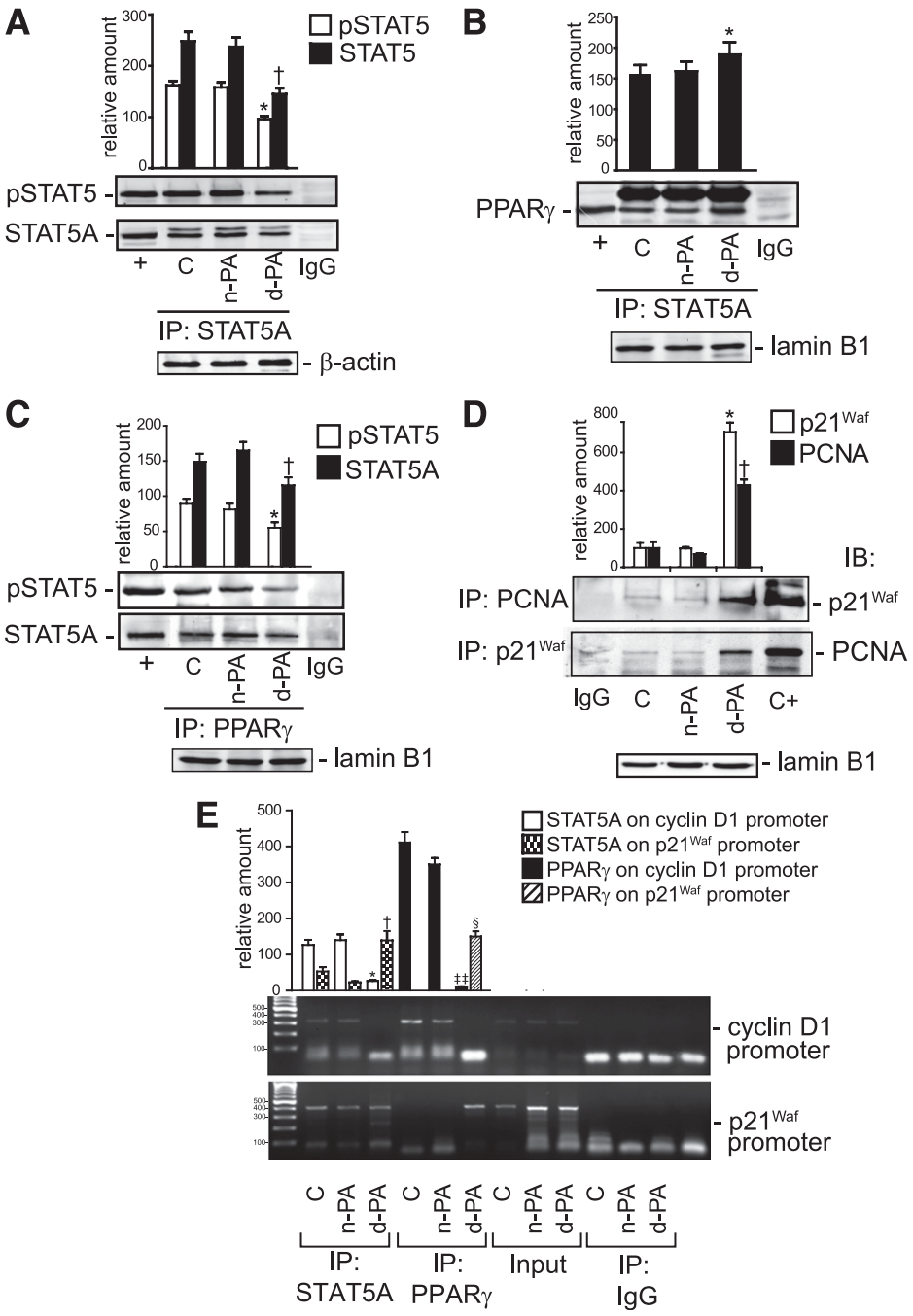

FIG. 4. The STAT5/PPARγ transcriptional complex binds to cyclin D1 or p21^{Waf} promoter depending on the requested biological response. *A*: Representative pSTAT5 and immunoprecipitated (IP) STAT5A expression in EPCs treated for 48 h as indicated; densitometric data, normalized to the corresponding β-actin values and expressed as mean + SD, are reported as relative amount expressed in arbitrary units (n = 9; *P < 0.05, pSTAT5: *d*-PA vs. C [control] and *n*-PA; †P < 0.05, STAT5A: *d*-PA vs. C and *n*-PA). *B*: Representative co-IP of PPARγ and STAT5A from nuclear extracts of EPCs treated for 48 h as indicated; densitometric data, normalized to the corresponding lamin B1 values and expressed as mean + SD, are reported as relative amount expressed in arbitrary units (n = 9; *P < 0.05, PPARγ: *d*-PA vs. C and *n*-PA). *C*: Representative co-IP of pSTAT5/STAT5A and PPARγ from nuclear extracts of EPCs treated for 48 h as indicated; densitometric data, normalized to the corresponding lamin B1 values and expressed as mean + SD, are reported as relative amount expressed in arbitrary units (n = 9; *P < 0.05, pSTAT5: *d*-PA vs. C and *n*-PA; †P < 0.05, STAT5A: *d*-PA vs. C and *n*-PA). *D*: Representative co-IP of p21^{Waf} and PCNA from nuclear extracts of EPCs treated for 48 h as indicated; densitometric data, normalized to the corresponding lamin B1 values and expressed as mean + SD, are reported as relative amount expressed in arbitrary units (n = 9; *P < 0.05, p21^{Waf}: *d*-PA vs. C and *n*-PA; †P < 0.05, PCNA: *d*-PA vs. C and *n*-PA). IL-3–stimulated ECs were used as positive control in *A–D* (+, *A–C*; C+, *D*). *E*: Representative ChIP analysis of PPARγ and STAT5A binding to cyclin D1 and p21^{Waf} promoters in EPCs treated as indicated at 15 days; densitometric data, normalized to the corresponding Input values and expressed as mean + SD, are reported as relative amount of PCR products (n = 9; *P < 0.05, STAT5A on cyclin D1 promoter: *d*-PA vs. C and *n*-PA; †P < 0.05, STAT5A on p21^{Waf} promoter: *d*-PA vs. C and *n*-PA; ‡‡P < 0.01, PPARγ on cyclin D1 promoter: *d*-PA vs. C and *n*-PA; §P < 0.05, PPARγ on p21^{Waf} promoter: *d*-PA vs. C and *n*-PA).

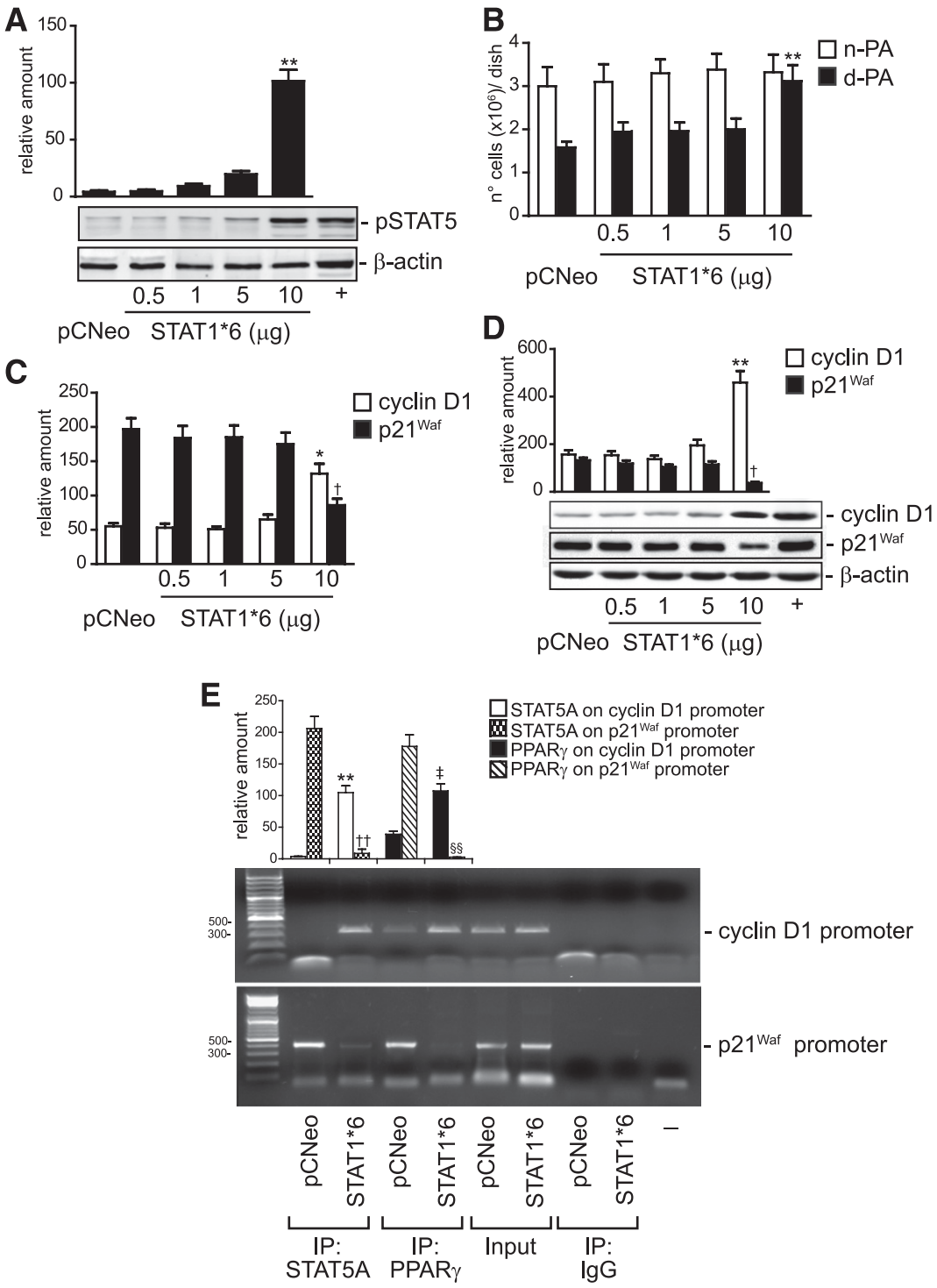

FIG. 5. The amount of activated STAT5 regulates EPC progression into the cell cycle. *A*: Representative WB and densitometric analysis of pSTAT5 protein content in EPCs transfected with different STAT1*6 plasmid concentrations or with the empty vector pCNeo and treated for 48 h with *d*-PA; densitometric data, normalized to the corresponding β-actin values and expressed as mean + SD, are reported as relative amount expressed in arbitrary units (n = 9; **P < 0.01, STAT1*6 10 μg vs. pCNeo, STAT1*6 0.5, 1, and 5 μg). IL-3–stimulated ECs were used as positive control (+). *B*: Proliferation of EPCs transfected with different STAT1*6 plasmid concentrations or with the empty vector pCNeo and treated for 48 h with *n*-PA or *d*-PA; data are expressed as mean + SD (n = 9; **P < 0.01, STAT1*6 10 μg *d*-PA–treated cells vs. pCNeo, STAT1*6 0.5, 1, 5, and 10 μg *n*-PA–treated cells and also vs. STAT1*6 0.5, 1, and 5 μg *d*-PA–treated cells). *C*: q-RT-PCR analysis of cyclin D1 and p21^{Waf} mRNA expression in EPCs transfected with different STAT1*6 plasmid concentration or with the empty vector pCNeo and treated for 48 h with *d*-PA; data, normalized to the corresponding GADPH mRNA and expressed as mean + SD, are reported as *m*-RNA relative amount expressed in arbitrary units (n = 9; *P < 0.05, cyclin D1: STAT1*6 10 μg *d*-PA–treated cells vs. pCNeo, STAT1*6 0.5, 1, and 5 μg *d*-PA–treated cells; †P < 0.05, p21^{Waf} STAT1*6 10 μg *d*-PA–treated cells vs. pCNeo, STAT1*6 0.5, 1, and 5 μg *d*-PA–treated cells). *D*: Representative WB and densitometric analysis of cyclin D1 and p21^{Waf} protein content in EPCs treated for 48 h as indicated; densitometric data, normalized to the corresponding β-actin values and expressed as mean + SD, are reported as relative protein amount expressed in arbitrary units (n = 9; **P < 0.01, cyclin D1: STAT1*6 10 μg *d*-PA–treated cells vs. pCNeo, STAT1*6 0.5, 1, and 5 μg *d*-PA–treated cells; †P < 0.05, p21^{Waf} STAT1*6 10 μg *d*-PA–treated cells vs. pCNeo, STAT1*6 0.5, 1, and 5 μg *d*-PA–treated cells). IL-3– and AGE-stimulated ECs were used as positive controls (+) for cyclin D1 or p21^{Waf}, respectively. *E*: Representative ChIP analysis of PPARγ and STAT5A binding to cyclin D1 and p21^{Waf} promoters in EPCs transfected with pCNeo or STAT1*6 vector and treated for 48 h with *d*-PA; densitometric data, normalized to the

Evidence has been provided that EPC mobilization is impaired in a diabetic setting (28). We demonstrate that *d*-PA prevented stromal cell–derived factor 1α (SDF-1α)–mediated EPC migration as well, suggesting that *d*-PA might also impair EPC–BM mobilization, a crucial event for EPC-mediated vascular protection. A reciprocal transcriptional cross-talk between STAT5 and PPARγ has been described in different tissue (48,49). Three different regulatory regions have been identified in the human STAT5 gene promoter (39). Regions I and II were recognized as putative STAT5A and STAT5B promoters, respectively, whereas region III has been described as a negative regulatory element shared by both genes. Region I and III contain different sequences denoted as A1, A2, and A3 (region I) and Inter1 and Inter2 (region III) (39). By interrogating NHRScan, two different PPREs were found in A3 and Inter2, further confirming that PPARγ can positively or negatively modulate STAT5A expression. Consistent with the low STAT5A content observed in response to *d*-PA, we first demonstrated that PPARγ binds to Inter2 to negatively regulate STAT5A expression. Moreover, we failed to detect changes in STAT5B expression, indicating that PPARγ binds to Inter2 to specifically regulate STAT5A expression.

Closed putative response elements for STAT5 and PPARγ are present in the promoter region of both $p21^{Waf}$ and cyclin D1 genes (22). We demonstrated that in *d*-PA–treated EPCs, both STAT5A and PPARγ bind to $p21^{Waf}$ promoter, indicating that although at low level of expression, STAT5A can form a transcriptional complex with PPARγ to induce the expression of $p21^{Waf}$. However, as the STAT5/PPARγ complex was also detected in *n*-PA–treated EPCs, we hypothesized that depending on the relative amount of STAT5A, the same transcriptional complex can target discrete genes. In fact, in agreement with the biological effect associated with *n*-PA treatment, we found that the STAT5/PPARγ complex stably binds to cyclin D1 gene promoter. $p21^{Waf}$ modulates cell-cycle progression by forming a complex with cyclins, cyclin-dependent protein kinases, and PCNA (40). It is known (40) that in absence of cyclins and cyclin-dependent protein kinases, $p21^{Waf}$ blocks progression into the cell cycle by physically interacting with PCNA, thus resulting in inhibition of PCNA-dependent activation of DNA polymerase δ. Our finding that $p21^{Waf}$–PCNA interaction could be only detected in *d*-PA–challenged EPCs indicates that such a mechanism might be crucial for regulating cell-cycle progression in our experimental conditions as well.

The role of STAT5 in controlling hematopoietic cell (23), EPC, and vascular cell (29) progression into the cell cycle has been extensively documented. A large body of evidence indicates that STAT5 regulates discrete biological functions by forming homodimeric (STAT5A/STAT5A or STAT5B/STAT5B) or heterodimeric (STAT5A/STAT5B, STAT5A/PPARγ, and STAT5/estrogen receptor) transcriptional complexes (22,50). However, whether and how the relative amount of individual transcriptional factor can modulate gene targeting and cell fate has not been investigated so far. In this study, we show that STAT5A content actually drives gene targeting and ultimately EPC fate. Deregulation of early hematopoiesis driven by PPARγ-mediated down-regulation of STAT5 has been described (23). In this study, we provide a proof of concept that, by regulating the relative amount of STAT5, *d*-PA controls gene targeting and BM-$CD117^+$ cell proliferation as well. The biological relevance of these results is supported by the findings that inhibition of *d*-PA–induced PPARγ activity rescued BM-$CD117^+$ cell colony formation. Moreover, as in mature ECs *d*-PA did not regulate STAT5 expression and cell-cycle progression, it is conceivable to assume that such a mechanism is relevant for immature cells only. This would be particularly relevant in specific clinical settings wherever re-entry into the cell cycle, to promote progenitor cell expansion, is needed.

EPCs contribute to maintain endothelial integrity, a crucial event to prevent vascular complications in diabetes (13,46). Evidence has been provided that hyperglycemia and its related metabolic disorders impair EPC bioavailability in a diabetic setting (13,46). In this study, we demonstrated how mechanistically *d*-PA and possibly a high level of NEFA plasma concentration in diabetic patients might contribute to EPC dysfunction (19,20,47). This possibility is also sustained by data obtained in EPCs subjected to high glucose and *d*-PA. Additional support to the role of *d*-PA–driven PPARγ transcriptional activity and EPC dysfunction is provided by the observation that by interfering with PPARγ activity, EPC vasculogenetic properties could be rescued. Plasma metabolomic profiling identifies as type 2 diabetes biomarkers PA, OA, and SA (2,3). We did not measure PA, OA, and SA plasma concentrations in diabetic patients. However, PA represents ~30% of total plasma NEFAs (6). This observation, together with the finding that when OA or SA diabetic concentrations were exploited in vitro we failed to detect significant effects on EPCs' functional capabilities, suggest that NEFA-mediated EPC toxic effect might depend on *d*-PA.

Pioglitazone treatment has been shown to improve the imbalance between endothelial damage and repair in a diabetic setting (15,44,45). However, whether this effect is direct or the result of its anti-inflammation and/or lipid modification is still debated (15). Our data demonstrated that pioglitazone protected *d*-EPCs from senescence and rescued their functional capability. However, this effect was not associated with changes in STAT5A and PPARγ content. This suggests that in vivo, the mechanisms involved in pioglitazone-mediated improvement of EPC bioavailability are much more complex than expected and require additional investigations.

Clinical data in nondiabetic patients sustain that favorable metabolic effect and cardiovascular protection are associated with mono- and polyunsaturated fatty acid administration (7). We found that physiological concentration of OA was able to rescue *d*-PA–induced EPC cell-cycle arrest. However, as OA plasma concentrations are increased in type 2 diabetes and contribute to the global increase of NEFAs (4,5), a potential deleterious effect of OA administration in diabetic patients has to be taken into consideration. As a proof of concept, metabolomic included OA among type 2 diabetes lipid biomarkers (3,5). Consistently, when *d*-OA concentrations were used in combination with *d*-PA, we failed to detect any protection, thus indicating that dietary interventions in diabetic patients should be targeted to

corresponding Input values and expressed as mean + SD, are reported as relative amount of PCR products ($n = 9$; **$P < 0.01$, STAT5A on cyclin D1 promoter STAT1*6 vs. pCNeo; ††$P < 0.01$, STAT5A on $p21^{Waf}$ promoter STAT1*6 vs. pCNeo; ‡$P < 0.05$ PPARγ on cyclin D1 promoter STAT1*6 vs. pCNeo; §§$P < 0.01$ PPARγ on $p21^{Waf}$ promoter STAT1*6 vs. pCNeo).

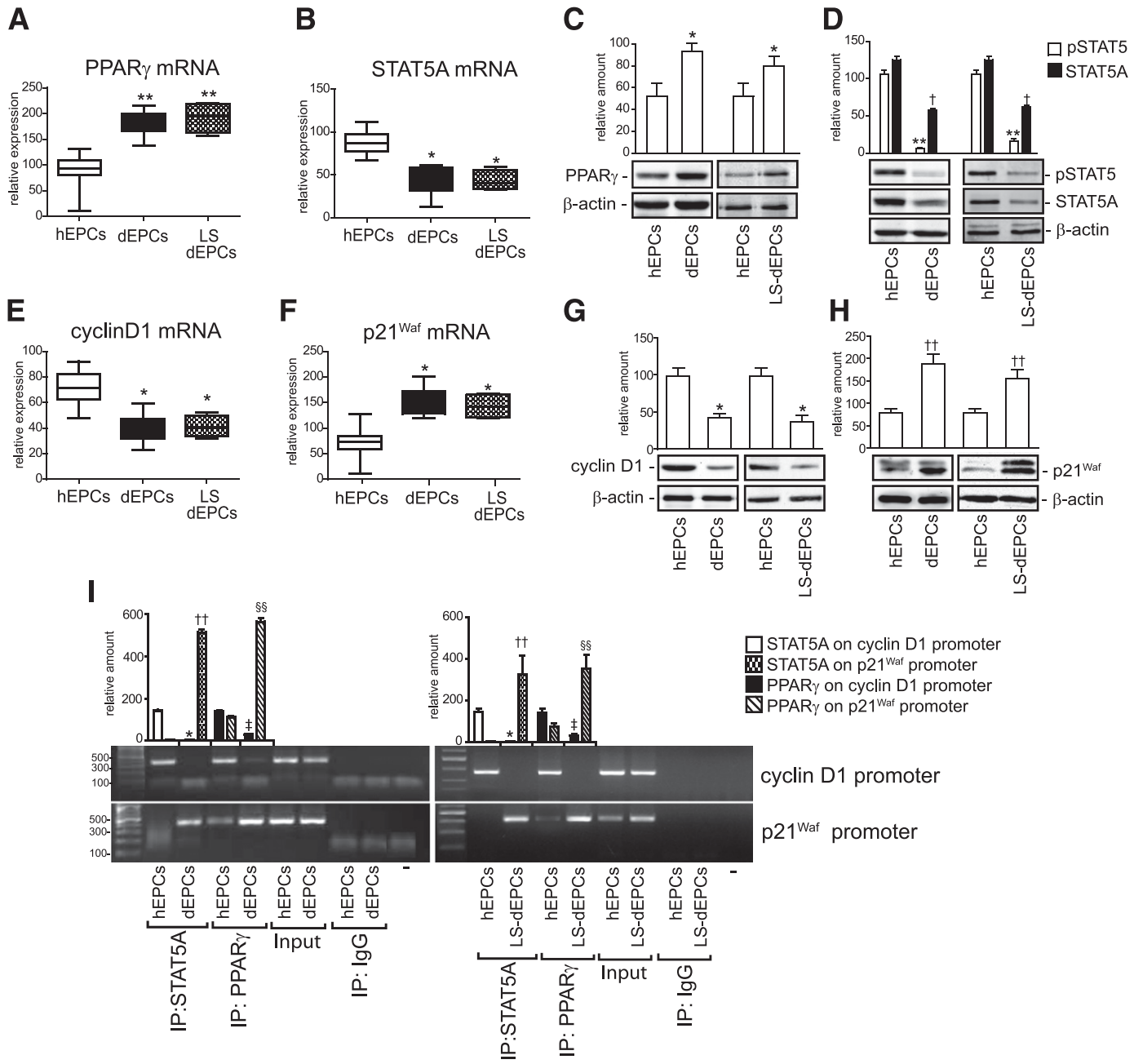

FIG. 6. The STAT5/PPARγ transcriptional complex binds to p21^{Waf} promoter in *d*-EPCs and LS-dEPCs. *A*: q-RT-PCR analysis of PPARγ mRNA expression in hEPCs, dEPCs, and LS-dEPCs (15 days of cultures); data normalized to the corresponding GADPH mRNA and depicted in box plot are reported as relative mRNA expression in arbitrary units (n = 14; **P < 0.01, dEPCs and LS-dEPCs vs. hEPCs). *B*: q-RT-PCR analysis of STAT5A mRNA expression in hEPCs, dEPCs and LS-dEPCs (15 days of culture); data normalized to the corresponding GADPH mRNA and depicted in box plot are reported as relative mRNA expression in arbitrary units (n = 14; *P < 0.05, dEPCs and LS-dEPCs vs. hEPCs). *C*: Representative WB and densitometric analysis of PPARγ protein content in hEPCs, dEPCs, and LS-dEPCs. Densitometric data, normalized to the corresponding β-actin values and expressed as mean + SD, are reported as relative amount expressed in arbitrary units (n = 14; *P < 0.05, dEPCs and LS-dEPCs vs. hEPCs). *D*: Representative WB and densitometric analysis of pSTAT5 and STAT5A protein content in hEPCs, dEPCs, and LS-dEPCs. Densitometric data, normalized to the corresponding β-actin values and expressed as mean + SD, are reported as relative amount expressed in arbitrary units (n = 14; **P < 0.01, pSTAT5 dEPCs and LS-dEPCs vs. hEPCs; †P < 0.05, STAT5 dEPCs and LS-dEPCs vs. hEPCs). *E*: q-RT-PCR analysis of cyclin D1 mRNA expression in hEPCs, dEPCs, and LS-dEPCs; data normalized to the corresponding GADPH mRNA and depicted in box plot are reported as relative mRNA expression in arbitrary units (n = 14; *P < 0.05, dEPCs and LS-dEPCs vs. hEPCs). *F*: q-RT-PCR analysis of p21^{Waf} mRNA expression in hEPCs, dEPCs, and LS-dEPCs; data, normalized to the corresponding GADPH mRNA and depicted in box plot, are reported as relative mRNA expression in arbitrary units (n = 14; *P < 0.05, dEPCs and LS-dEPCs vs. hEPCs). *G*: Representative WB and densitometric analysis of cyclin D1 protein content in hEPCs, dEPCs, and LS-dEPCs. Densitometric data, normalized to the corresponding β-actin values and expressed as mean + SD, are reported as relative amount expressed in arbitrary units (n = 14; *P < 0.05, cyclinD1 dEPCs and LS-dEPCs vs. hEPCs). *H*: Representative WB and densitometric analysis of p21^{Waf} protein content in hEPCs, dEPCs, and LS-dEPCs. Densitometric data, normalized to the corresponding β-actin values and expressed as mean + SD, are reported as relative amount expressed in arbitrary units (n = 14; ††P < 0.01, p21^{Waf} dEPCs and LS-dEPCs vs. hEPCs). *I*: Representative ChIP analysis of PPARγ and STAT5A binding to cyclin D1 and p21^{Waf} promoters in hEPCs, dEPCs, and LS-dEPCs; densitometric data, normalized to the corresponding Input values and expressed as mean + SD, are reported as relative amount of PCR products (n = 14; *P < 0.05, STAT5A on cyclin D1 promoter dEPCs and LS-dEPCs vs. hEPCs; ††P < 0.01, STAT5A on p21^{Waf} promoter dEPCs and LS-dEPCs vs. hEPCs; ‡P < 0.05, PPARγ on cyclin D1 promoter dEPCs and LS-dEPCs vs. hEPCs; §§P < 0.01, PPARγ on p21^{Waf} promoter dEPCs and LS-dEPCs vs. hEPCs).

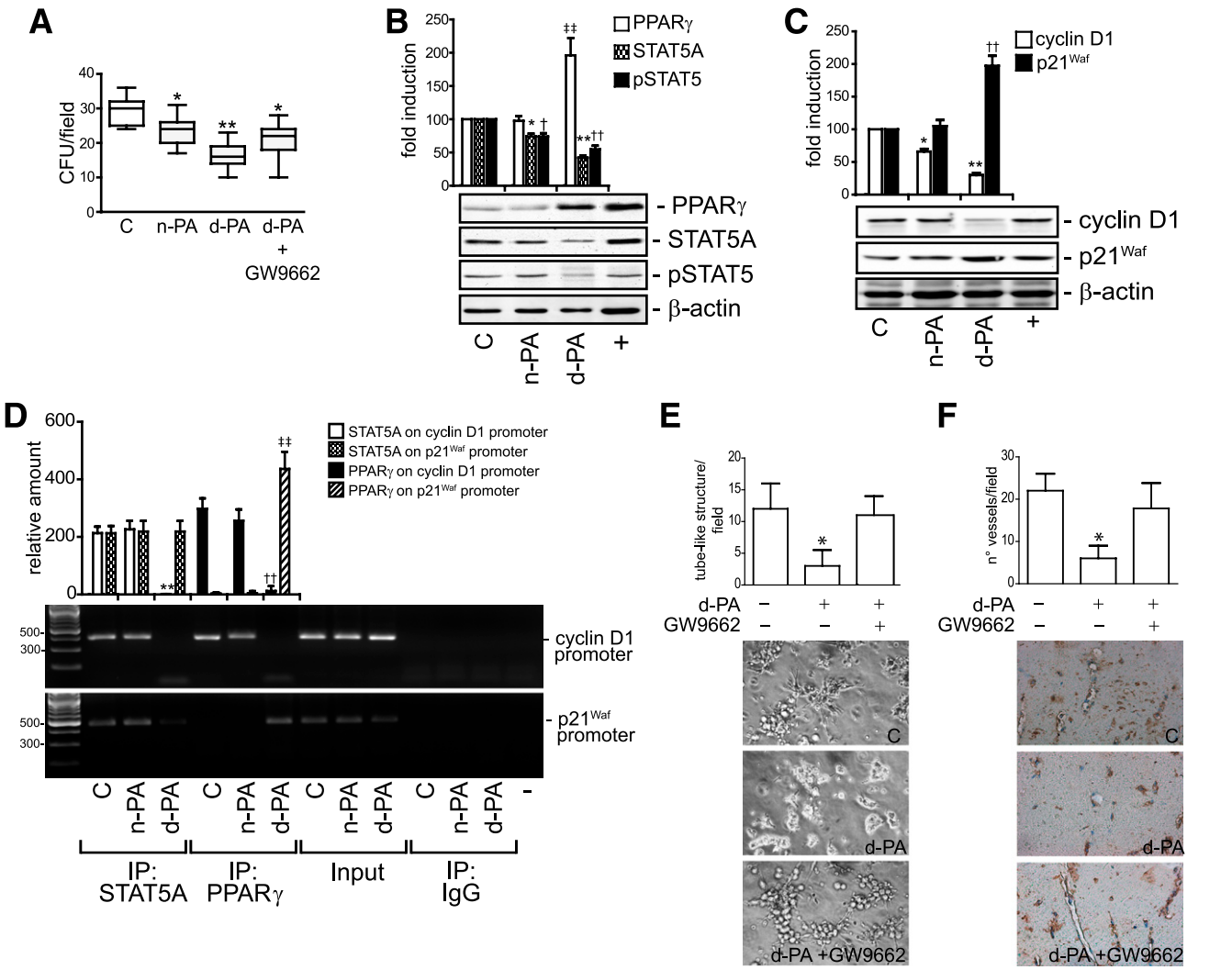

FIG. 7. Effects of *d*-PA on hematopoietic progenitor cells and on EPC vasculogenic capability. *A*: Number of colonies formed by CD117/c-kit$^+$ cells treated for 15 days as indicated. In selected experiments, GW9662, a specific PPARγ inhibitor, was added; data are expressed as mean ± SD (n = 6; *P < 0.05, *n*-PA and *d*-PA + GW9662 vs. C [control]; **P < 0.01 *d*-PA vs. C, *n*-PA, and *d*-PA + GW9662). *B*: Representative WB and densitometric analysis of PPARγ, STAT5, and pSTAT5 protein content in cells treated as above indicated; densitometric data, normalized to the corresponding β-actin values and expressed as mean + SD, are reported as fold induction relative to control values arbitrary set as 100 (n = 9; *P < 0.05, STAT5A *n*-PA vs. C; **P < 0.01, STAT5A *d*-PA vs. C; †P < 0.05, pSTAT5 *n*-PA vs. C; ††P < 0.01, pSTAT5 *d*-PA vs. C; ‡‡P < 0.01, PPARγ *d*-PA vs. C and *n*-PA). IL-3–stimulated ECs were used as positive control (+). *C*: Representative WB and densitometric analysis of cyclin D1 and p21^{Waf} protein content in cells treated for 15 days as indicated; densitometric data, normalized to the corresponding β-actin values and expressed as mean + SD, are reported as fold induction relative to control values arbitrary set as 100 (n = 9; *P < 0.05, cyclin D1: *n*-PA vs. C; **P < 0.01, cyclin D1: *d*-PA vs. C; ††P < 0.01, p21^{Waf}: *d*-PA vs. C and *n*-PA). IL-3– and AGE-stimulated ECs were used as positive controls (+) for cyclin D1 or p21^{Waf}, respectively. *D*: Representative ChIP analysis of PPARγ and STAT5A binding to cyclin D1 and p21^{Waf} promoters in cells treated for 15 days as indicated; densitometric data, normalized to the corresponding Input values and expressed as mean + SD, are reported as relative amount of PCR products (n = 6; **P < 0.01, STAT5A on cyclin D1 promoter *d*-PA vs. C and *n*-PA; ††P < 0.01, PPARγ on cyclin D1 promoter *d*-PA vs. C and *n*-PA; ‡‡P < 0.01, PPARγ on p21^{Waf} promoter *d*-PA vs. C and *n*-PA). *E*: Tube-like structure formation assay in basement Matrigel matrix of EPCs treated as indicated. Data are expressed as mean + SD (n = 3; **d*-PA vs. C and GW9662 + *d*-PA). *F*: In vivo vasculogenic capability of EPCs treated as indicated. Data are expressed as mean + SD (n = 3; **d*-PA vs. C and GW9662 + *d*-PA). Prelabeled [fluorescent dye 5- (and 6-)carboxyfluorescein diacetate succinimidyl ester] human EPCs were used. Anti-fluorescein/Oregon Green polyclonal antibody and horseradish peroxidase–labeled anti-rabbit antibody were used to selectively detect injected cells (brown-stained cells in the image).

normalize NEFA concentrations rather than merely suggest OA supplementation.

In conclusion, these data first demonstrate how mechanistically *d*-PA can contribute to EPC and BM-derived hematopoietic dysfunction and provide the rationale to exploit such a target for novel therapeutic strategies.

ACKNOWLEDGMENTS

This work was supported by grants from the Italian Association for Cancer Research, Ministero dell'Università e della Ricerca Scientifica progetto Progetti di Rilevante Interesse Nazionale, and Regione Piemonte (Ricerca Sanitaria Finalizzata) (to M.F.B.).

No potential conflicts of interest relevant to this article were reported.

A.T. was involved in EPC isolation and characterization; treatments and transfections; WB, ChIP, IP, and CoIP experiments; genomic DNA isolation and sequence amplification; luciferase assay; bioinformatic analysis; and statistical analysis. G.T. was involved in BM-derived hematopoietic cell isolation and PCRs. A.R. was involved in construct

generation and performed site-directed mutagenesis and CFU formation assay. P.D. was involved in the in vivo experiments. C.O. performed PCRs. P.C. was involved in blood sample recovering. M.F.B. was involved in study conception and design and writing the manuscript. M.F.B. is the guarantor of this work and, as such, had full access to all the data in the study and takes responsibility for the integrity of the data and the accuracy of the data analysis.

The authors thank Prof. Ezio Ghigo (Department of Medical Sciences, University of Torino) for clinical support.

REFERENCES

1. Li X, Xu Z, Lu X, et al. Comprehensive two-dimensional gas chromatography/time-of-flight mass spectrometry for metabonomics: Biomarker discovery for diabetes mellitus. Anal Chim Acta 2009;633:257–262
2. Friedrich N. Metabolomics in diabetes research. J Endocrinol 2012;215: 29–42
3. Liu L, Li Y, Guan C, et al. Free fatty acid metabolic profile and biomarkers of isolated post-challenge diabetes and type 2 diabetes mellitus based on GC-MS and multivariate statistical analysis. J Chromatogr B Analyt Technol Biomed Life Sci 2010;878:2817–2825
4. Boden G. Free fatty acids, insulin resistance, and type 2 diabetes mellitus. Proc Assoc Am Physicians 1999;111:241–248
5. Yi LZ, He J, Liang YZ, Yuan DL, Chau FT. Plasma fatty acid metabolic profiling and biomarkers of type 2 diabetes mellitus based on GC/MS and PLS-LDA. FEBS Lett 2006;580:6837–6845
6. Stumvoll M, Nurjhan N, Perriello G, Dailey G, Gerich JE. Metabolic effects of metformin in non-insulin-dependent diabetes mellitus. N Engl J Med 1995;333:550–554
7. Nolan CJ, Larter CZ. Lipotoxicity: why do saturated fatty acids cause and monounsaturates protect against it? J Gastroenterol Hepatol 2009;24:703–706
8. Chinetti G, Fruchart JC, Staels B. Peroxisome proliferator-activated receptors (PPARs): nuclear receptors at the crossroads between lipid metabolism and inflammation. Inflamm Res 2000;49:497–505
9. Auwerx J, Martin G, Guerre-Millo M, Staels B. Transcription, adipocyte differentiation, and obesity. J Mol Med (Berl) 1996;74:347–352
10. Gervois P, Torra IP, Fruchart JC, Staels B. Regulation of lipid and lipoprotein metabolism by PPAR activators. Clin Chem Lab Med 2000;38: 3–11
11. Komers R, Vrána A. Thiazolidinediones—tools for the research of metabolic syndrome X. Physiol Res 1998;47:215–225
12. Toyama K, Nakamura T, Kataoka K, et al. Telmisartan protects against diabetic vascular complications in a mouse model of obesity and type 2 diabetes, partially through peroxisome proliferator activated receptor-γ-dependent activity. Biochem Biophys Res Commun 2011;410: 508–513
13. Fadini GP, Avogaro A. It is all in the blood: the multifaceted contribution of circulating progenitor cells in diabetic complications. Exp Diabetes Res 2012;2012:742976
14. Duan SZ, Usher MG, Mortensen RM. Peroxisome proliferator-activated receptor-gamma-mediated effects in the vasculature. Circ Res 2008;102: 283–294
15. Wang CH, Ting MK, Verma S, et al. Pioglitazone increases the numbers and improves the functional capacity of endothelial progenitor cells in patients with diabetes mellitus. Am Heart J 2006;152:1051.e1-e8
16. Robinson E, Grieve DJ. Significance of peroxisome proliferator-activated receptors in the cardiovascular system in health and disease. Pharmacol Ther 2009;122:246–263
17. Jaumdally RJ, Lip GY, Patel JV, MacFadyen RJ, Varma C. Effects of coronary artery disease and percutaneous intervention on the cardiac metabolism of nonesterified fatty acids and insulin: Implications of diabetes mellitus. J Intern Med 2009;265:689–697
18. Hill JM, Zalos G, Halcox JP, et al. Circulating endothelial progenitor cells, vascular function, and cardiovascular risk. N Engl J Med 2003;348:593–600
19. Guo WX, Yang QD, Liu YH, Xie XY, Wang-Miao, Niu RC. Palmitic and linoleic acids impair endothelial progenitor cells by inhibition of Akt/eNOS pathway. Arch Med Res 2008;39:434–442
20. Jiang H, Liang C, Liu X, et al. Palmitic acid promotes endothelial progenitor cells apoptosis via p38 and JNK mitogen-activated protein kinase pathways. Atherosclerosis 2010;210:71–77
21. Schoonjans K, Staels B, Auwerx J. The peroxisome proliferator activated receptors (PPARS) and their effects on lipid metabolism and adipocyte differentiation. Biochim Biophys Acta 1996;1302:93–109
22. Dentelli P, Trombetta A, Togliatto G, et al. Formation of STAT5/PPARgamma transcriptional complex modulates angiogenic cell bioavailability in diabetes. Arterioscler Thromb Vasc Biol 2009;29:114–120
23. Prost S, Le Dantec M, Augé S, et al. Human and simian immunodeficiency viruses deregulate early hematopoiesis through a Nef/PPARgamma/STAT5 signaling pathway in macaques. J Clin Invest 2008;118:1765–1775
24. Yoder MC, Mead LE, Prater D, et al. Redefining endothelial progenitor cells via clonal analysis and hematopoietic stem/progenitor cell principals. Blood 2007;109:1801–1809
25. Togliatto G, Trombetta A, Dentelli P, Rosso A, Brizzi MF. MIR221/MIR222-driven post-transcriptional regulation of P27KIP1 and P57KIP2 is crucial for high-glucose- and AGE-mediated vascular cell damage. Diabetologia 2011;54:1930–1940
26. Svedberg J, Björntorp P, Smith U, Lönnroth P. Free-fatty acid inhibition of insulin binding, degradation, and action in isolated rat hepatocytes. Diabetes 1990;39:570–574
27. Cham BE, Knowles BR. A solvent system for delipidation of plasma or serum without protein precipitation. J Lipid Res 1976;17:176–181
28. Togliatto G, Trombetta A, Dentelli P, et al. Unacylated ghrelin rescues endothelial progenitor cell function in individuals with type 2 diabetes. Diabetes 2010;59:1016–1025
29. Zeoli A, Dentelli P, Rosso A, et al. Interleukin-3 promotes expansion of hemopoietic-derived CD45+ angiogenic cells and their arterial commitment via STAT5 activation. Blood 2008;112:350–361
30. Sadowski HB, Shuai K, Darnell JE Jr, Gilman MZ. A common nuclear signal transduction pathway activated by growth factor and cytokine receptors. Science 1993;261:1739–1744
31. Onishi M, Nosaka T, Misawa K, et al. Identification and characterization of a constitutively active STAT5 mutant that promotes cell proliferation. Mol Cell Biol 1998;18:3871–3879
32. Weiner MP, Gackstetter T, Costa GL, Bauer JC, Kretz KA. Site-directed mutagenesis using PCR. In *Molecular Biology: Current Innovations and Future Trends*. Griffin AM, Griffin HG, Eds. Norfolk, United Kingdom, Horizon Scientific Press, 1995, p. W1–W2
33. Uberti B, Dentelli P, Rosso A, Defilippi P, Brizzi MF. Inhibition of β1 integrin and IL-3Rβ common subunit interaction hinders tumour angiogenesis. Oncogene 2010;29:6581–6590
34. Clore JN, Allred J, White D, Li J, Stillman J. The role of plasma fatty acid composition in endogenous glucose production in patients with type 2 diabetes mellitus. Metabolism 2002;51:1471–1477
35. Kastorini CM, Panagiotakos DB. Dietary patterns and prevention of type 2 diabetes: from research to clinical practice; a systematic review. Curr Diabetes Rev 2009;5:221–227
36. Hu W, Ross J, Geng T, Brice SE, Cowart LA. Differential regulation of dihydroceramide desaturase by palmitate versus monounsaturated fatty acids: implications for insulin resistance. J Biol Chem 2011;286: 16596–16605
37. Lehrke M, Lazar MA. The many faces of PPARgamma. Cell 2005;123:993–999
38. Sauma L, Stenkula KG, Kjølhede P, Strålfors P, Söderström M, Nystrom FH. PPAR-gamma response element activity in intact primary human adipocytes: effects of fatty acids. Nutrition 2006;22:60–68
39. Crispi S, Sanzari E, Monfregola J, et al. Characterization of the human STAT5A and STAT5B promoters: evidence of a positive and negative mechanism of transcriptional regulation. FEBS Lett 2004;562:27–34
40. Waga S, Hannon GJ, Beach D, Stillman B. The p21 inhibitor of cyclin-dependent kinases controls DNA replication by interaction with PCNA. Nature 1994;369:574–578
41. Kliewer SA, Sundseth SS, Jones SA, et al. Fatty acids and eicosanoids regulate gene expression through direct interactions with peroxisome proliferator-activated receptors alpha and gamma. Proc Natl Acad Sci USA 1997;94:4318–4323
42. Fajas L, Auboeuf D, Raspé E, et al. The organization, promoter analysis, and expression of the human PPARgamma gene. J Biol Chem 1997;272: 18779–18789
43. Margeli A, Kouraklis G, Theocharis S. Peroxisome proliferator activated receptor-gamma (PPAR-gamma) ligands and angiogenesis. Angiogenesis 2003;6:165–169
44. Esposito K, Maiorino MI, Di Palo C, et al. Effects of pioglitazone versus metformin on circulating endothelial microparticles and progenitor cells in patients with newly diagnosed type 2 diabetes—a randomized controlled trial. Diabetes Obes Metab 2011;13:439–445

45. Gensch C, Clever YP, Werner C, Hanhoun M, Böhm M, Laufs U. The PPAR-gamma agonist pioglitazone increases neoangiogenesis and prevents apoptosis of endothelial progenitor cells. Atherosclerosis 2007;192:67–74
46. Menegazzo L, Albiero M, Avogaro A, Fadini GP. Endothelial progenitor cells in diabetes mellitus. Biofactors 2012;38:194–202
47. Artwohl M, Lindenmair A, Sexl V, et al. Different mechanisms of saturated versus polyunsaturated FFA-induced apoptosis in human endothelial cells. J Lipid Res 2008;49:2627–2640
48. Meirhaeghe A, Fajas L, Gouilleux F, et al. A functional polymorphism in a STAT5B site of the human PPAR gamma 3 gene promoter affects height and lipid metabolism in a French population. Arterioscler Thromb Vasc Biol 2003;23:289–294
49. Shipley JM, Waxman DJ. Down-regulation of STAT5b transcriptional activity by ligand-activated peroxisome proliferator-activated receptor (PPAR) alpha and PPARgamma. Mol Pharmacol 2003;64:355–364
50. Wang Y, Cheng CH. ERalpha and STAT5a cross-talk: interaction through C-terminal portions of the proteins decreases STAT5a phosphorylation, nuclear translocation and DNA-binding. FEBS Lett 2004;572:238–244